Near-Inertial Oscillations of a Barotropic Vortex: Trapped Modes and Time Evolution

STEFAN G. LLEWELLYN SMITH

Department of Applied Mathematics and Theoretical Physics, University of Cambridge, Cambridge, United Kingdom

(Manuscript received 14 November 1997, in final form 26 May 1998)

ABSTRACT

Amplified motions in vortices have been observed in Gulf Stream rings and over seamounts. This paper uses the near-inertial oscillation approximation to model near-inertial motions in the presence of a barotropic vortical background flow. The resulting trapped modes are calculated: there is always at least one such mode, but higher modes may exist and these are obtained. The characteristics of the trapped mode depend on the quantity $\Gamma/f_0R_n^2$ where Γ is the circulation (integrated vorticity) of the ring, f_0 is the local Coriolis frequency, and R_n is the nth Rossby radius of deformation, which may be interpreted as a combined measure of the vertical length scale and stratification. Asymptotic expressions are presented for the frequency of the gravest radial mode for strong and weak vortices. The calculated frequencies are compared to previous results, and good agreement is obtained. The initial value problem is also studied: the contribution of the trapped modes to the evolution of the near-inertial wave field is calculated, as is the contribution due to the continuous spectrum. The long time behavior of the continuous spectrum decays like $(\ln t)^{-1}$ and takes different forms in the vortex core and far from the vortex.

1. Introduction

Warm core rings are the most spectacular oceanic example of coherent structures with strongly negative core vorticity. Because ray-tracing calculations show that internal waves are trapped inside regions of negative vorticity (Kunze 1985) one anticipates that these vortices might contain localized near-inertial activity. Indeed, the observations of Kunze and Lueck (1986), Kunze (1986), and Kunze et al. (1995, KST hereafter) show convincing signatures of trapped, near-inertial modes in a warm core ring. KST also contains a theoretical investigation of the near-inertial trapped modes of an axisymmetric barotropic vortex. However, the calculations of KST neglect regular singularities in the coefficients of the equation they solve, neglect interactions with certain mean-flow terms outside the vortex, and implement an incorrect matching condition across the edge of the vortex. More recent work (Kunze and Boss 1998, KB hereafter) has been necessary to vindicate the main theoretical conclusions of KST. Kunze and Toole (1997) have studied the trapped near-inertial modes over Fieberling Guyot using a similar model.

In this paper we use the near-inertial oscillation (NIO) approximation developed by Young and Ben Jelloul (1997, YBJ hereafter) to examine the near-inertial modes on a barotropic, axisymmetric vortex. Because the NIO approximation is a reduction of the linearized primitive equations, the time-dependent equations for NIOs in rings can be cast in a straightforward form. The resulting equations do not suffer from the mathematical inconsistencies of the original KST analysis, and lead to a simple formulation of the time-dependent problem. The eigenproblem for trapped modes may be solved in a similar fashion to KB, although there are some important differences, as will be seen. In addition, however, the time-dependent problem is solved. This leads to interesting information on the role of the propagating and the trapped modes in the evolution of the system. An important point is that the NIO approximation is based on a multiple timescale approximation and does not assume separation of spatial scales between the geostrophic flow (the ring) and the near-inertial waves (the eigenmode). Thus, results based on the NIO approximation are not limited to modes whose spatial scale is much smaller than that of the vortex. In fact, we will find interesting examples of weakly trapped modes with radial decay scales of many vortex diameters. This does mean, however, that results obtained using the approximation must be examined to check that the predicted slow timescale is not too close to the inertial period, which would invalidate the approximation.

The outline of the paper is as follows. Section 2 outlines the formulation of the problem using the theory of YBJ. Section 3 solves the dispersion relation for the Rankine vortex, both in nondimensional form and also

Corresponding author address: Dr. Stefan G. Llewellyn Smith, Dept. of Applied Mathematics & Theoretical Physics, University of Cambridge, Silver Street, Cambridge CB3 9EW, United Kingdom.
E-mail: sgls1@damtp.cam.ac.uk

taking into account a model of ocean stratification. The latter results are compared to the results of KB. Section 4 examines the trapped modes for a family of vorticity profiles that are more realistic than the Rankine vortex and identifies asymptotic properties of the dispersion relation that hold for all ring profiles. Section 5 examines the initial value problem of the evolution of the trapped mode, given a spatially uniform excitation, Finally, section 6 discusses and summarizes the results of the paper. Mathematical results not central to the paper are given in the appendix.

2. Formulation

a. The NIO approximation

We start with the NIO equation of YBJ. The wave variables are expressed in terms of a complex field, $\mathcal{A}(x, y, z, t)$, by

$$u + iv = e^{-if_0t}L\mathcal{A}, \tag{1}$$

$$w = -(f_0^2/N^2)\mathcal{A}_{z\xi}e^{-if_0t} + \text{c.c.}, \tag{2}$$

$$b = if_0\mathcal{A}_{z\xi}e^{-if_0t} + \text{c.c.}, \tag{3}$$

$$p = if_0\mathcal{A}_{\xi}e^{-if_0t} + \text{c.c.} \tag{4}$$

The differential operators ∂_ξ and L are defined by

$$\mathcal{A}_\xi \equiv \frac{1}{2}(\mathcal{A}_x - i\mathcal{A}_y), \qquad L\mathcal{A} \equiv (f_0^2N^{-2}\mathcal{A}_z)_z. \tag{5}$$

Using (1)–(4), the leading-order dynamical variables associated with the near-inertial oscillation can be obtained from $\mathcal{A}$. The complex field $\mathcal{A}$ evolves according to the NIO equation of YBJ

$$L\mathcal{A}_t + \frac{\partial(\Psi, L\mathcal{A})}{\partial(x, y)} + \frac{i}{2}f_0\nabla^2\mathcal{A} + \frac{i}{2}ZL\mathcal{A} = 0, \tag{6}$$

where Ψ is the geostrophic streamfunction and $Z = \nabla^2\Psi$ is the geostrophic vorticity. Throughout this paper, $\nabla^2 \equiv \partial_x^2 + \partial_y^2$ is the horizontal Laplacian. The equation for the wavefield $\mathcal{A}$ is linear, and we shall take $\mathcal{A}$ to have value 1 at the origin.

b. Projection onto vertical normal modes

We confine our attention to barotropic flows, $\Psi_z = 0$. This is a dramatic simplification of the highly baroclinic structure of the vortices that have been observed, and many physical processes are therefore lost. However, in doing so, we can follow the analysis of KST in order to make the resulting problem analytically tractable; in particular it is now possible to project onto vertical normal modes. Using the notation of Gill (1984), the Sturm–Liouville problem associated with the linear operator L is

$$L\hat{p}_n + f_0^2c_n^{-2}\hat{p}_n = 0, \tag{7}$$

where the eigenvalue, $c_n = f_0R_n$, is the speed of mode n and R_n is the Rossby radius of mode n. The functions $\hat{p}_n(z)$ are vertical normal modes. The Sturm–Liouville problem (7) defines the Rossby radius R_n, which may be related in the case of constant stratification N to a vertical wavelength λ_z by

$$R_n = \frac{\lambda_z N}{2\pi f_0}. \tag{8}$$

The field $\mathcal{A}$ is represented as

$$\mathcal{A}(x, y, z, t) = \sum_{n=1}^{\infty} \mathcal{A}_n(x, y, t)\hat{p}_n(z), \tag{9}$$

and each modal amplitude satisfies the Schrödinger-like equation

$$\mathcal{A}_{nt} + \frac{\partial(\Psi, \mathcal{A}_n)}{\partial(x, y)} + \frac{i}{2}Z\mathcal{A}_n = \frac{i\hbar_n}{2}\nabla^2\mathcal{A}_n, \tag{10}$$

where

$$\hbar_n \equiv f_0R_n^2, \tag{11}$$

is the "dispersivity" of mode n. The terms in (10) have obvious physical interpretations: advection, frequency shift, and, on the right-hand side, wave dispersion.

c. The eigenproblem for an axisymmetric vortex

For a barotropic radially symmetric eddy, $\Psi(r)$, with azimuthal velocity $V = \Psi_r$, (10) reduces to

$$\mathcal{A}_{nt} + \Omega\mathcal{A}_{n\theta} + \frac{i}{2}Z\mathcal{A}_n - \frac{i}{2}\hbar_n\nabla^2\mathcal{A}_n = 0, \tag{12}$$

where $\Omega \equiv V/r$ and $Z = \Psi_{rr} + r^{-1}\Psi_r$. This equation has an energy integral that may be obtained by multiplying by $\mathcal{A}_n^*$ and taking the real part. The result is

$$\mathcal{E}_{nt} + \Omega\mathcal{E}_{n\theta} + \nabla\cdot\mathbf{F}_n = 0, \tag{13}$$

where the energy density of the nth vertical mode is $\mathcal{E}_n = \frac{1}{2}\mathcal{A}_n\mathcal{A}_n^*$ and the energy density flux is given by

$$\mathbf{F}_n = \frac{i}{2}\hbar_n(\mathcal{A}_n^*\nabla\mathcal{A}_n - \mathcal{A}_n\nabla\mathcal{A}_n^*). \tag{14}$$

The advective term $\Omega\mathcal{E}_{n\theta}$ in (13) cannot result in an energy flux to infinity. Requiring that $\mathbf{F}_n \to 0$ as $r \to \infty$ is the boundary condition for trapped near-inertial modes.

For a radial vortex, solutions of the form $\mathcal{A}_n = e^{i(m\theta-\omega t)}A_n(r)$ may be sought. The resulting eigenproblem for ω is

$$A'' + \frac{1}{r}A' + \left[\frac{2}{\hbar}\left(\omega - m\Omega - \frac{1}{2}Z\right) - \frac{m^2}{r^2}\right]A = 0. \tag{15}$$

We have now lightened notation by suppressing the subscript n on A and $\hbar$. The boundary condition on the eigenproblem above is that A decays faster than $r^{-1/2}$ as $r \to \infty$ so that $\mathbf{F}$ vanishes at great distances from the

vortex. (This requirement distinguishes the discrete, trapped modes of the vortex from the continuum of radiation modes.)

Multiplying (15) by rA^* and integrating leads to the relation

$$2\omega\int_0^\infty r|A|^2\,dr = \hbar\int_0^\infty r|A'|^2\,dr + m^2\hbar\int_0^\infty \frac{|A|^2}{r}\,dr + \int_0^\infty (2m\Omega + Z)r|A|^2\,dr. \tag{16}$$

Because we are limiting our attention to trapped modes with rapid decay, terms such as $[rA'A^*]_0^\infty$ arising from the integration by parts are zero. This result shows that the eigenfrequency, ω, is real. Then, without loss of generality, one can take A to be real.

In addition, if $(\omega^{(1)}, A^{(1)})$ and $(\omega^{(2)}, A^{(2)})$ are both solutions of (15), then one can obtain the orthogonality relation

$$[\omega^{(1)} - \omega^{(2)}]\int_0^\infty rA^{(1)}(r)A^{(2)}(r)\,dr = 0; \tag{17}$$

that is, radial eigenfunctions with distinct eigenvalues are orthogonal. Equation (17), together with the orthogonality relations for the vertical and azimuthal structure functions can be used to project an initial condition onto the three-dimensional eigenfunctions (see section 5).

We now nondimensionalize the problem. We take the vortex to have radius a and circulation Γ. We now define a nondimensional radial coordinate by $\eta \equiv r/a$. The vortex is then specified by giving the vorticity in the form

$$Z(r) = \frac{\Gamma}{a^2}\Delta(\eta). \tag{18}$$

The profile function, $\Delta(\eta)$, is normalized by

$$\int_0^\infty \Delta(\eta)\eta\,d\eta = \frac{1}{2\pi}, \tag{19}$$

so that Γ is, in fact, the total circulation of the vortex. In this paper, the frequency ω of the normal mode of the NIO wavefield is a departure from the inertial frequency f_0. The actual physical frequency is $f_0 + \omega$.

d. Comparison with alternate formulations

Our formulation of the eigenproblem differs from the earlier works of KST and KB in several respects. First, we use a Cartesian representation of the velocity field, namely $u + iv$, whereas KST and KB use the radial component of the velocity, u_r, as the independent variable (following Brink 1989, 1990). This difference produces ambiguity in the definition of the azimuthal wavenumber: because

$$u_r = \mathrm{Re}[e^{-i\theta}(u + iv)], \tag{20}$$

it follows that our azimuthal wavenumber $m = 0$ corresponds to the azimuthal wavenumber -1 of KST and KB.

Despite the axisymmetry of the vortex, the Cartesian form, $u + iv$, is a natural representation of the linearly polarized NIO modes observed by KST. Specifically, Fig. 14 of KST shows that the inertially backrotated wave phase, which corresponds to the phase of $\mathcal{A}$, does not vary around the ring. In essence, this means that if $\mathcal{A}$ is decomposed into azimuthal modes of the form $e^{im\theta}$, then only the $m = 0$ mode is present and $\mathcal{A} = \mathcal{A}(r, t)$.

It may seem that the distinction between u_r and $u + iv$ is an unimportant formality but there are attendant differences in the physical interpretation of the results that are confusing. The main issue concerns the possible Doppler shift produced by the term $\Omega\mathcal{A}_{n\theta}$ in (12). For our $m = 0$ mode, this advective term vanishes exactly, and so there is no Doppler shift. However, if one uses u_r as the independent variable, then for the same mode, the advective term is nonzero and this leads to the distinction that KST draw between the Lagrangian and Eulerian frequencies.

As a simple illustration of these different interpretations consider a solid-body flow with $(U, V) = \Omega(-y, x)$; the vorticity is 2Ω. For disturbances with very large spatial scale, the pressure gradient is negligible and, using the Cartesian representation, one has

$$\frac{Du}{Dt} - (\Omega + f_0)v = 0, \tag{21}$$

$$\frac{Dv}{Dt} + (\Omega + f_0)u = 0, \tag{22}$$

where $D/Dt = \partial_t - \Omega y\partial_x + \Omega x\partial_y = \partial_t + \Omega\partial_\theta$ is the convective derivative. The solution of (22) is

$$(u + iv) = e^{-i(f_0+\Omega)t}. \tag{23}$$

Thus, the frequency shift is Ω, or half of the vorticity of the solid-body flow. The advective terms in D/Dt vanish because u and v in (23) do not depend on the spatial coordinates; that is, there is no Doppler shift in this Cartesian representation.

Alternatively, one can solve this problem using cylindrical coordinates with the independent variables

$$u_r = u\cos\theta + v\sin\theta, \tag{24}$$

$$u_\theta = -u\sin\theta + v\cos\theta. \tag{25}$$

In cylindrical coordinates the equations of motion are

$$\frac{Du_r}{Dt} - (2\Omega + f_0)u_\theta = 0, \tag{26}$$

$$\frac{Du_\theta}{Dt} + (2\Omega + f_0)u_r = 0, \tag{27}$$

and the solution is

$$(u_r, u_\theta) = \{\cos[\theta + (f_0 + \Omega)t],\ -\sin[\theta + (f_0 + \Omega)t]\}. \tag{28}$$

In (26) and (27) the shift in the inertial frequency is 2Ω, but the advective term is nonzero and its contribution (a ''Doppler shift'') cancels half of the apparent frequency shift. This leads to the distinction that KST and KB draw between the intrinsic frequency, $\omega_i = f_0 + 2\Omega$, and the Eulerian frequency, $\omega_E = \omega_i + n\Omega$ [for the solution in (28) the azimuthal wavenumber is $n = -1$].

Of course the two representations are completely equivalent; that is, (23) and (28) are the same. This example shows that the distinction between the intrinsic frequency and the Eulerian frequency depends on which equivalent representation of the velocity field one happens to use. In ray-tracing problems, such as those discussed by Kunze (1985), the notion of a Doppler shift is well defined and useful. But in the present context it makes no sense to assign a Doppler shift to a trapped modal structure (as opposed to a propagating plane wave).

3. Trapped modes in a Rankine vortex

We follow KST by considering the Rankine vortex, specified by

$$\Delta(\eta) = \begin{cases} \pi^{-1} & \text{for } \eta < 1 \\ 0 & \text{for } \eta > 1, \end{cases} \tag{29}$$

as an initial example. Our strategy is to first solve the Rankine case in some detail and then turn to the more realistic examples with smooth vorticity profiles. Many, but not all, features of the Rankine case are representative of the general case.

a. The $m = 0$ case

The easiest case, and the one which corresponds most closely to the observations of KST, is $m = 0$. In nondimensional form, the $m = 0$ eigenproblem is

$$A_{\eta\eta} + \frac{1}{\eta}A_\eta + \frac{2a^2\omega}{\hbar}A - \frac{\Gamma}{\hbar}\Delta(\eta)A = 0. \tag{30}$$

For $\eta > 1$, $\Delta = 0$. A bound state solution is only possible for $\omega < 0$, that is, only if the frequency of the mode is subinertial. For $\eta < 1$, $\Delta = 1/\pi$, and we anticipate that the coefficient of the undifferentiated term in (30) must be positive; that is, $2a^2\omega - \Gamma/\pi > 0$. The two conditions $\omega < 0$ and $2a^2\omega - \Gamma/\pi > 0$ together imply that the vortex must have negative circulation $\Gamma < 0$ for trapped waves to exist. Hence trapped normal modes are only possible for anticyclonic vortices, such as rings (see KST).

The solution of (30) for $\eta < 1$ is

$$A \propto J_0\left(\eta\sqrt{\frac{2a^2\omega}{\hbar} - \frac{\Gamma}{\pi\hbar}}\right). \tag{31}$$

For $\eta > 1$, the solution is

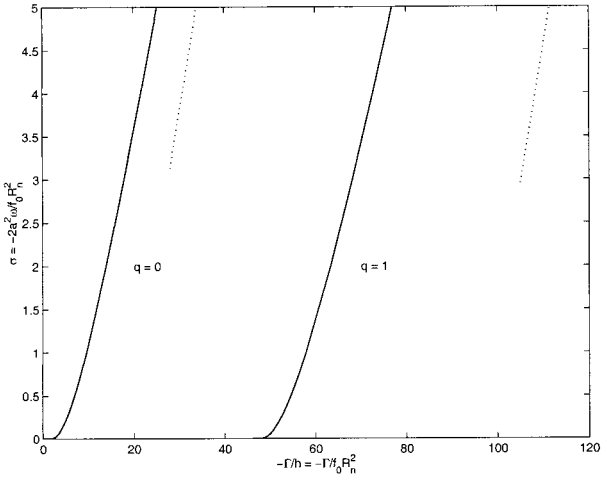

FIG. 1. The first two eigenbranches obtained from the eigenvalue relation (33), plotted as solid curves. The abscissa is the nondimensional vortex strength parameter $-\Gamma/\hbar$ and the ordinate is the nondimensional frequency $\sigma = -2a^2\omega/\hbar$. The dotted lines show the large-σ behavior of the eigenbranches from (36). The next eigenbranch, $q = 2$, starts around $-\Gamma/\hbar \approx 150$.

$$A \propto K_0\left(\eta\sqrt{\frac{2a^2|\omega|}{\hbar}}\right). \tag{32}$$

The matching condition at $\eta = 1$ is obtained by matching pressure and radial velocity as in KB. In the NIO approximation, the complex velocity is proportional to $\mathcal{A}_n$ [because of (7)] whereas pressure is proportional to $\mathcal{A}_{n\xi}$. In polar coordinates, therefore, the radial velocity is continuous if $A(r)$ is continuous and the pressure is continuous if $A'(r)$ is continuous. The two conditions on A and its derivative lead to the eigenvalue relation

$$\sqrt{2a^2|\omega|/\hbar}\sqrt{2a^2\omega/\hbar - \Gamma/\pi\hbar} - \frac{J_1(\sqrt{2a^2|\omega| - \Gamma/\pi\hbar})}{J_0(\sqrt{2a^2|\omega|/\hbar - \Gamma/\pi\hbar})} = \frac{K_1(\sqrt{2a^2|\omega|/\hbar})}{K_0(\sqrt{2a^2|\omega|/\hbar})}. \tag{33}$$

This equation may be solved numerically to give the eigenvalue relation for the nondimensional frequency $\sigma > 0$, defined by

$$\sigma \equiv -\frac{2a^2\omega}{\hbar}, \tag{34}$$

as a function of the nondimensional ''vortex strength,'' $-\Gamma/\hbar > 0$. Figure 1 shows the first two branches, labeled $q = 0$ and $q = 1$, of the eigenrelation in the $(-\Gamma/\hbar, \sigma)$ plane. The branches originate with $\sigma = 0$ at circulation values $-\Gamma/\hbar = \pi j_{1,q}^2$, where $j_{1,q}$ is the qth zero of J_1.[1]

[1] The integer index q starts at $q = 0$; we use the convention that the ''zeroth'' zero of J_1 is $j_{1,0} = 0$. Then, as in Abramowitz and Stegun (1965), $j_{1,1} \approx 3.83$, etc.

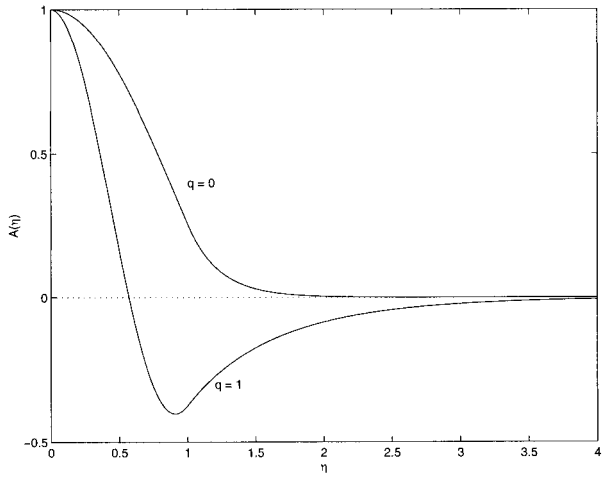

FIG. 2. The velocity amplitude $A(r)$ [chosen to have $A(0) = 1$] for the two radial modes supported by a Rankine vortex with $-\Gamma/\hbar = 60$. The vortex has radius $\eta = 1$.

We may note that the form of the curves of Fig. 1 is independent of the the value of R_n since the abscissa and ordinate both scale with R_n^{-2}.

The gravest radial mode is the $q = 0$ branch emerging from the origin in Fig. 1. Consequently, very weak vortices (i.e., vortices with $0 < -\Gamma/\hbar \ll 1$) have a single, trapped, near-inertial mode. In this limit, the approximate solution of the eigenvalue relation (33) is

$$\sigma \sim e^{4\pi\hbar/\Gamma} \ll 1. \tag{35}$$

The eigenfrequency σ is "exponentially small" in the vortex strength parameter $-\Gamma/\hbar$; this explains why the $q = 0$ eigencurve in Fig. 1 is so "flat" near the origin. The mode is weakly trapped because the radial decay scale, l_K, of the modified Bessel function K_0 in (32) is $l_K \approx a/\sqrt{\sigma} \gg a$. That is, most of the eigenfunction is outside the core of the vortex.

As the strength of the vortex increases and we proceed up the $q = 0$ curve in Fig. 1, the mode becomes tightly bound to the vortex core. Also, as $-\Gamma/\hbar$ increases, new modes with more radial structure appear: $q = 1$ and so on. At their birth on the abscissa of Fig. 1, the modes have $\sigma \ll 1$, and consequently the new modes are weakly trapped. But as $|\Gamma/\hbar|$ increases the higher modes also become tightly bound to the vortex core. Figure 2 shows the two radial modes supported by a vortex with $-\Gamma/\hbar = 60$; the corresponding values of the nondimensional frequency parameter σ are 1.38 and 15.32.

In the limit of large σ and $\Gamma/\hbar$, the eigenvalue relation is approximately linear and given by

$$\sigma \sim -\frac{\Gamma}{\pi\hbar} - j_{0,q+1}^2, \tag{36}$$

where $j_{0,q+1}$ is the $(q + 1)$th zero of the Bessel function J_0. This linear relation is shown by the dotted straight lines in Fig. 1. The agreement is not good for the relatively small values of σ in Fig. 1; however, the dotted lines do show the eventual $\sigma \gg 1$ behavior of the eigenbranches.

TABLE 1. Physical parameters: the first five are parameters for the Gill model buoyancy profile (in fact N_{mix} is derived from the previous four), and the last four, which relate to the vortex and its surroundings, are taken from KST.

Description	Abbreviation	Value
Depth of ocean	H	4200 m
Depth of mixed layer	H_{mix}	50 m
Length scale of deep N^2 profile	z_0	4330 m
Stratification parameter	s	2.5 m s^{-1}
Buoyancy frequency at base of mixed layer	N_{mix}	0.01392 s^{-1}
Coriolis parameter	f_0	10^{-4} s^{-1}
Radius of vortex	a	43 km
Core vorticity	ζ_c	$-f_0/4$
Circulation of vortex	$\Gamma = \pi\zeta_c a^2$	-1.45×10^5 m^2 s^{-1}

b. *The $m \neq 0$ case*

The results of the previous section apply only to the special case $m = 0$, that is, modes with no azimuthal structure, such as those observed by KST. We made an unsuccessful effort to find solutions of (15) with $m \neq 0$. We did prove rather easily that there are no solutions with $m < 0$. But the case $m > 0$ remains open. We do not know if such solutions exist, nor can we prove that they do not exist.

c. *Trapped modes in the presence of a model buoyancy profile*

Figure 1 presents the solution of the eigenproblem in a compact nondimensional form. However, it is difficult from this figure to estimate the variables with the most immediate physical meaning. Therefore, at the risk of some redundancy, we will consider a specific example and find the eigenfrequencies in dimensional variables. This approach has the advantage that one can make an a posteriori assessment of the validity of the NIO approximation.

We must first solve the vertical mode eigenproblem in (7) and obtain the Rossby radius and modal dispersivity $\hbar_n = f_0 R_n^2$. We use the buoyancy profile of Gill (1984):

$$N(z) = \begin{cases} 0 & \text{if } H - H_{\text{mix}} < z < H \\ s/(z_0 - z) & \text{if } 0 < z < H - H_{\text{mix}} \end{cases} \tag{37}$$

($z = 0$ is the bottom of the ocean). The parameters for the buoyancy profile are given in Table 1: $\hbar_n$ decreases rapidly (like n^{-2}) as n increases. Thus, the vortex strength parameter, $-\Gamma/\hbar_n$, becomes larger as the vertical mode number increases.

The characteristics of the vortex are chosen to match Fig. 5 of KST and are given in Table 1. The resulting

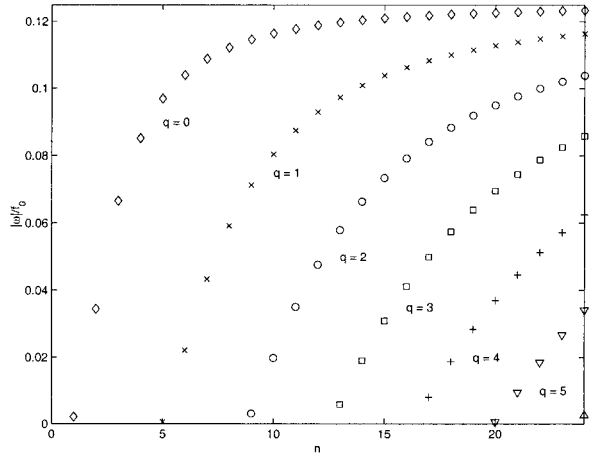

FIG. 3. Modal frequency $|\omega|/f_0$ as a function of vertical mode number n for the first five radial eigenmodes. (The azimuthal mode number is $m = 0$ in all cases.) The modes with $q \geq 1$ exist for sufficiently large n (i.e., only for sufficiently large $\Gamma/\hbar_n$). As n increases, all of the eigencurves asymptote to $|\zeta_c|/2f_0$ (1/8 in the figure above).

profile is a simple approximation to what was measured by KST.[2]

Figure 3 shows the absolute value of the modal frequency, $|\omega|/f_0$, as a function of the vertical mode number n for the first few radial eigenmodes. This eigenrelation has the form

$$\omega_{n,q} = -\frac{\hbar_n}{2a^2} F_q\left(-\frac{\Gamma}{\hbar_n}\right), \tag{38}$$

where the $F_q > 0$ are the nondimensional functions displayed in Fig. 1 for $q = 0$ and $q = 1$. The eigenfrequency of the mode with vertical mode number n and radial mode number q is $\omega_{n,q} < 0$. (The azimuthal mode number is $m = 0$ in all cases.) As the vertical mode number n increases, there are more trapped radial modes. Also, because the eigenfrequencies are negative, all of the trapped modes have slightly subinertial frequencies. Figure 3 shows that new radial modes arise at the vertical mode numbers 1, 5, 9, 13, 17, 20, and 25.

In terms of dimensional variables, the approximate dispersion relation (36) is

$$\omega_{n,q} \approx \frac{1}{2}\zeta_c + \frac{\hbar_n}{2a^2} j^2_{0,q+1}, \tag{39}$$

where ζ_c is the constant vorticity in the core of the Rankine vortex. The approximation above shows that the modal frequencies, $\omega_{n,q}$, saturate at $\zeta_c/2$ for large n. Thus, the largest value of $|\omega_{n,q}|$ is always less than $|\zeta_c/2|$. The timescale separation assumption made in YBJ is that $|\omega|/f_0 \ll 1$ so that, in this problem, one requires that $|\zeta_c|/2f_0 \ll 1$. This condition is verified a posteriori for the parameters in Fig. 3, for which $|\omega_{n,q}|/f_0 < 1/8 \ll 1$.

d. Comparison with the results of KB

Kunze and Boss calculated the frequencies of trapped near-inertial oscillations in the presence of a background barotropic azimuthal flow, which is meant to model the warm core rings of KST and also the strong vortex cap observed above Fieberling Guyot. The parameters for the warm core ring and Fieberling Guyot are given in Table 2. We shall use the same values to be able to compare results.

The results obtained so far may now be applied to the warm core ring and to Fieberling Guyot. We shall not use any model for the buoyancy profile, but rather calculate the dispersivity from the parameters of KB. The resulting value of $\hbar$ will not correspond to a vertical mode as such, but will give a numerical value appropriate to the measurements as reported by KB.

The analysis of KB is in terms of a vertical wavelength λ_z, which we shall relate to the dispersivity $\hbar$ through [cf. (8)]

$$\hbar = \left(\frac{\lambda_z}{2\pi}\right)^2 \frac{N^2}{f_0}. \tag{40}$$

As in KB, only the gravest radial mode ($q = 0$) is considered and the vorticity distribution is taken to be the Rankine vortex. The governing parameter in the eigenrelation (33) is then

$$\frac{\Gamma}{\hbar} = \frac{4\pi^2\Gamma}{\lambda_z^2 N^2} = \frac{4\pi^3 f_0 \zeta_c a^2}{\lambda_z^2 N^2}. \tag{41}$$

For each radial mode, the dispersion relation is monotonic (see Fig. 1), and hence it suffices to consider the extremal values of $\Gamma/\hbar$ to obtain bounds for the frequency of each mode. High values of σ, that is, frequencies farther away from the inertial frequency, are obtained for large values of ζ_c and small values of N^2 and λ_z, and vice versa.

For the warm core ring, these parameters lead to extremal values for $|\Gamma|/\hbar$ of 78 and 1086. This corresponds to a dimensional frequency in the range $0.95f_0 < \omega_E = f_0 + \omega < 0.98f_0$. This is the Eulerian frequency of KST and KB. The most subinertial frequency corresponds to the larger value of $|\Gamma|/\hbar$, that is, to the stronger vortex. One advantage of the current representation is that it is easy to provide bounds for the frequency of the trapped mode, given the range of the physical parameters. The analysis of KST and KB is in terms of the effective Coriolis frequency, $f_{\text{eff}} \equiv f_0 + \zeta_c$. The ratios ω_E/f_{eff} and ω_i/f_{eff}, where ω_i is the intrinsic or Lagrangian frequency of KST, depend both on $\Gamma/\hbar$ and on ζ_c. In fact, the Eulerian frequency ratio ω_E/f_{eff} increases monotonically with $\Gamma/\hbar$ with extremal values

[2] The Coriolis frequency however is taken to be 10^{-4} s^{-1}: the small difference from the actual value at the latitude of the warm core ring (9.4×10^{-5} s^{-1}) has no importance for the results of this section.

TABLE 2. Physical parameters for a warm core ring and Fieberling Guyot (taken from KB).

Description	Abbreviation	Warm core ring	Fieberling Guyot[a]
Coriolis parameter	f_0	9.4×10^{-5} s^{-1}	8×10^{-5} s^{-1}
Radius of vortex/Guyot	a	43 km	5–7 km
Scaled core vorticity	$-\zeta_c/f_0$	0.04–0.1	0.45–0.52
Vertical wavelength	λ_z	96–200 m	170–220 m
Buoyancy frequency	N	4.5–5.1 ($\times 10^{-3}$ s^{-1})	4–5 ($\times 10^{-3}$ s^{-1})

[a] Data originally from Kunze and Toole (1997).

$\omega_E = (1.024–1.056) f_{\text{eff}}$. This is within 1% of the range $(1.022–1.062) f_{\text{eff}}$ calculated by KB (in terms of the factor in front of f_{eff}). The intrinsic frequency, on the other hand, decreases with ζ_c for fixed $\Gamma/\hbar$ and increases with $\Gamma/\hbar$ for fixed ζ_c. As a consequence its extremal values do not necessarily correspond to the extremal values of $\Gamma/\hbar$ and ζ_c and must be obtained as a two-parameter problem.

Figure 4 shows the solution envelope. It is very similar to Fig. 5 of KST and Fig. 2 of KB. The present solutions also match smoothly across $r = a$. The outer and inner radial wavelengths of KB become $l_K = 2\pi a\sigma^{-1/2}$ and $l_J = 2\pi a(-\sigma - \Gamma/\pi\hbar)^{-1/2}$. The inner radial wavelength has the range 118–136 km while the outer has the range 15–59 km. The KB values are 118–136 km and 15–60 km, respectively, and the agreement is excellent.

The magnitude of the quantity $\Gamma/\hbar$ suggests that the asymptotic expression (39) should be a good approximation to the actual frequency. In fact, the leading order term in (39), $\frac{1}{2}\zeta_c$, is good to better than 0.3%. Hence, for these large values of $-\Gamma/\hbar$, the value of the core vorticity gives the frequency of the trapped mode.

The same calculation for Fieberling Guyot using the values of Table 2, which give two possible values for the core radius, leads to a range of $7.4 < |\Gamma|/\hbar < 22.3$ for a radius of 5 km and to a range of 14.5–43.7 for the 7-km radius. The corresponding frequency ranges are $(0.85–0.95) f_0$ and $(0.81–0.90) f_0$, respectively. These ranges indicate that the predicted frequency is too far from f_0 for the NIO approximation to hold. The same remarks as before about the dependence of the frequencies expressed in terms of f_{eff} apply, further complicated by the existence of two different core radii. The range of the Eulerian frequency is $(1.719–1.764) f_{\text{eff}}$ for the 5-km radius and $(1.630–1.679) f_{\text{eff}}$ for the 7-km radius. The agreement in this case with the results of KB is only good to about 18%. The resulting eigenfunction envelopes in Fig. 5 are similar to those of KB, but are smooth since the appropriate matching condition for the NIO problem leads to continuous A and A', unlike the KB matching condition. The range of inner wavelengths is 18–24 km for the 5-km core and 23–28 km for the 7-km core, compared to the 22–34-km values of KB.

The asymptotic relation (39) does not hold for these parameter values. The measured K_1 tidal frequency of $0.933 f_0$ lies within the calculated range for the 5-km radius core. Taking the larger values of λ_z and ζ_c and

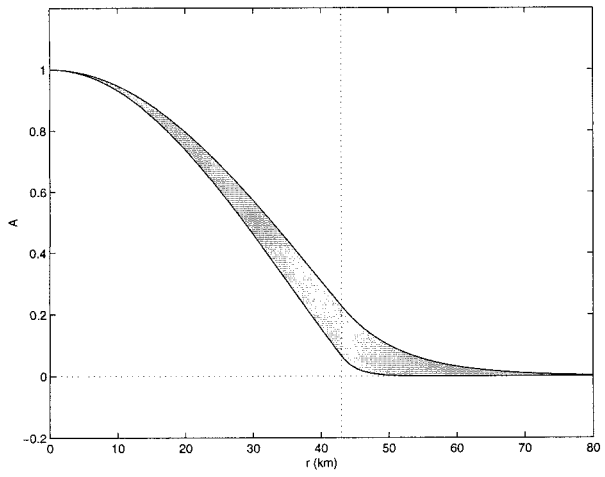

FIG. 4. Solution envelope, $A(r)$, for the warm core ring considered in KST and KB. The upper bounding curve corresponds to the smaller value of $|\Gamma|/\hbar$ and is less trapped than the lower curve, which corresponds to the larger value of $|\Gamma|/\hbar$. The dotted line corresponds to the edge of the vortex at 43 km.

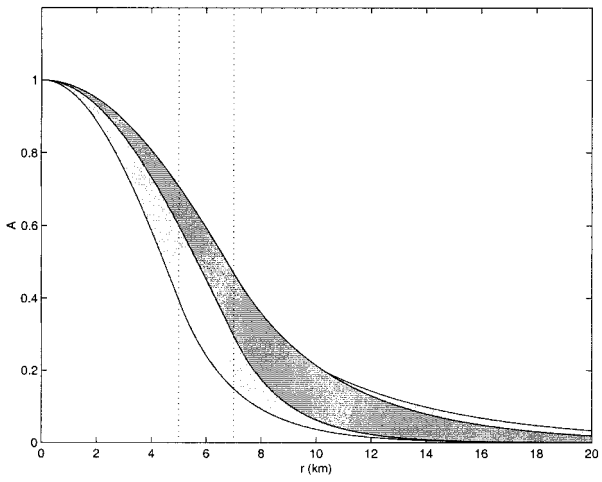

FIG. 5. Solution envelope, $A(r)$, for Fieberling Guyot, as considered by KB. The inner envelope corresponds to the 7-km core radius, the outer envelope to the 5-km core radius. Both radii are shown as dotted lines. As in Fig. 4, the upper limit of each envelope corresponds to the smaller value of $|\Gamma|/\hbar$ and the lower to the larger value of $|\Gamma|/\hbar$.

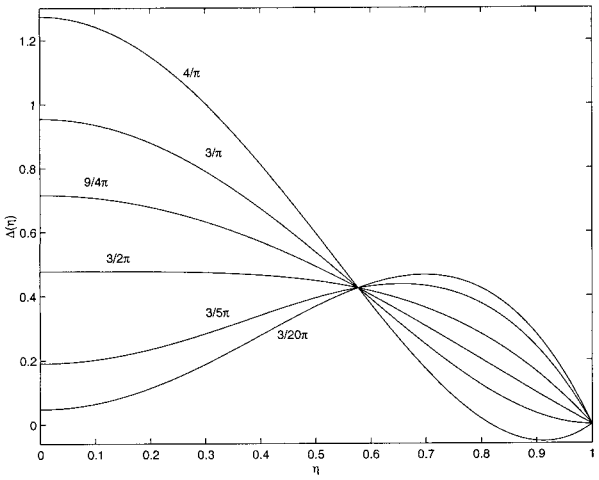

FIG. 6. Six members of the quartic vorticity-profile family $\Delta(\eta)$. The value of $\Delta_0 = \Delta(0)$ is given next to each curve.

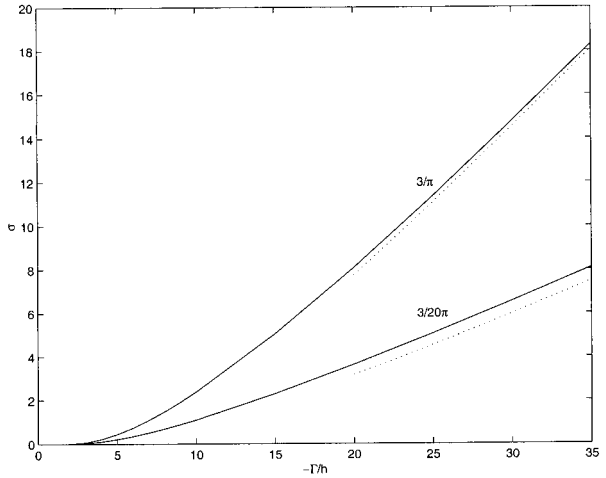

FIG. 7. Eigenvalue curves for the first radial eigenmode ($q = 0$) of the quartic family (solid lines). The value of Δ_0 is indicated next to the eigenvalue curves. The asymptotic approximations (44) and (45) are the dotted curves.

the smaller value of N leads to a theoretical value of $0.9454 f_0$, which is within 1.4% of the observed value.

We emphasize that the results in Figs. 4 and 5, as in KB, apply only to the gravest radial and azimuthal mode $q = 0$ and $m = 0$, respectively. The argument has often been made that large-scale forcing will dominantly excite this mode. In section 5 we provide a critical assessment of this assumption.

4. Trapped modes in smooth vorticity profiles

a. A family of quartic vorticity profiles

We now turn to the near-inertial eigenstructure for vortices with spatially varying core vorticity. We obtain numerical results for an illustrative family of vorticity profiles and compare these to some asymptotic results that apply to arbitrary profiles. The profiles that we consider are given by

$$\Delta(\eta) = \Delta_0(1 - 4\eta^2 + 3\eta^4) + \frac{6}{\pi}\eta^2(1 - \eta^2) \quad (42)$$

for $\eta < 1$ and 0, otherwise (see Fig. 6). The profiles above form a one-parameter (Δ_0) family, normalized so that (19) is satisfied. If the vorticity at the origin, Δ_0, is greater than $3/\pi$, the vorticity changes sign in the interval (0, 1). Such profiles have been observed although they are presumably barotropically unstable. The results for these vortices are the same as for those with Δ_0 in the range $(3/2\pi, 3/\pi)$. However for $\Delta_0 < 3/2\pi$, $\Delta''(0) > 0$, with the vorticity increasing from Δ_0 up to a maximum Δ_m, the results do change. The important difference is the presence of a maximum in negative vorticity away from the origin. These cases are similar to the measured vorticity profile of KST (their Fig. 5). Dewar (1987) argued that winter cooling might be responsible for forming such structures. It turns out that the case with a noncentral Δ_m has some interesting qualitative differences from the Rankine vortex of section 3.

The eigenfunctions take the form (32) for $\eta > 1$ since the vorticity vanishes beyond the core of the vortex. Inside the vortex, (30) is solved numerically. Using a trial value of ω, the resulting solutions are matched onto each other, and the procedure is repeated until A and A' are continuous (which is the appropriate matching condition as discussed previously), yielding the eigenfrequency ω. The first eigenbranch, $q = 0$ is shown in Fig. 7 for two representative members of the family, one with maximum vorticity at the origin ($\Delta_0 = 3/\pi$ and hence monotonically decaying) and one with maximum vorticity in the core of the vortex but not at the origin ($\Delta_0 = 3/20\pi$, in which case the maximum in vorticity is at $\eta \cong 0.7$). The dotted curves show the asymptotic behavior for large $|\Gamma|/\hbar$. The agreement is not as good for the latter profile as for the former.

Figure 8 shows the birth of the second eigenmode for the quartic profile with $\Delta = 3/5\pi$. The appearance of new eigenmodes is very similar to the case of the Rankine vortex; the second branch emerges at $-\Gamma/\hbar \sim 58$ (as opposed to 46 in the Rankine case).

Figure 9 shows the radial modes for the quartic family for the same values of Δ_0 as Fig. 7, with $-\Gamma/\hbar = 20$. The maximum of A moves away from $\eta = 0$ more slowly than the maximum of the vorticity profile to which it corresponds. This shows that the vorticity minimum must be displaced a fair way from the center of the vortex for the trapped mode to have a clear maximum away from the core. Figure 10 quantifies this by showing η_m, the value of η where $\Delta(\eta)$ has its maximum against η_A, the value of η where $A(\eta)$ achieves its maximum. For the quartic family, the maximum in A does not move off the axis until $\eta_m > 0.65$.

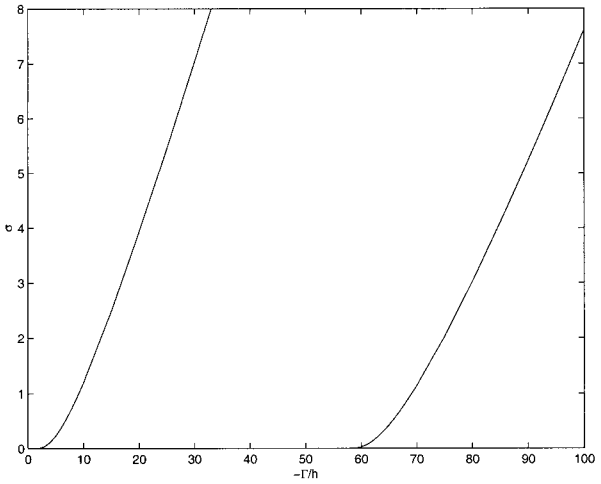

FIG. 8. First two eigenbranches of the quartic profile with $\Delta_0 = 3/5\pi$. The second branch appears at around $-\Gamma/\hbar \approx 58$.

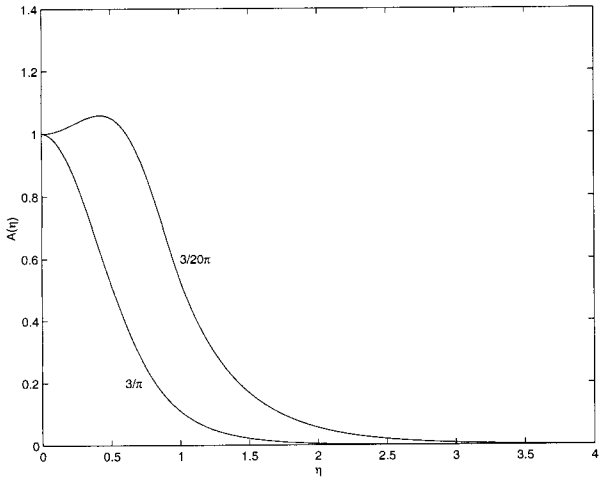

FIG. 9. The velocity amplitudes $A(r)$ of the lowest ($q = 0$) radial modes of the quartic family with $-\Gamma/\hbar = 20$. The values of Δ_0 characterizing each mode are shown next to the curve.

b. Asymptotic results: The q = 0 branch near the origin

A remarkable aspect of Fig. 7 is that the eigenvalues coincide near the origin of the $(\sigma, -\Gamma/\hbar)$ plane. This suggests that the structure of the $q = 0$ eigenbranch becomes independent of the vorticity profile as σ tends to 0. The analysis in appendix A confirms this expectation by showing that, in this limit,

$$\sigma \sim e^{4\pi\hbar/\Gamma}. \tag{43}$$

Physically, when $\sigma \ll 1$, the mode is weakly trapped and only ''feels'' the total circulation Γ of the vortex; roughly speaking, the weakly trapped mode ''sees'' the vortex as a point singularity of strength Γ.

c. Asymptotic results: The q = 0 branch for large σ and large −Γ/ħ

The behavior of the eigencurves for the gravest radial mode for large $|\Gamma|/\hbar$ and large σ depends on whether Δ_m is located at the origin (e.g., the curve $\Delta_0 = 3/\pi$ in Fig. 6) or away from the origin (e.g., the curve $\Delta_0 = 3/5\pi$ in Fig. 6).

For Δ_m at $\eta = 0$, and σ and $|\Gamma|/\hbar$ both large, the analysis in appendix B shows that the approximate eigenvalue relation is

$$\sigma \sim \frac{\Gamma}{\hbar}\Delta_0 - \sqrt{\frac{\Gamma}{\hbar}2\Delta''(0)} - \frac{1}{6}\frac{\Delta^{iv}(0)}{\Delta''(0)}. \tag{44}$$

Notice that Δ_0 is positive while Γ and $\Delta''(0)$ are both negative.

For vorticity profiles with $\Delta_0 < \Delta_m$ [or equivalently $\Delta''(0) > 0$], the approximate eigenrelation is

$$\sigma \sim -\frac{\Gamma}{\hbar}\Delta_m - \sqrt{-\frac{\Gamma}{\hbar}\frac{\Delta''(\eta_m)}{2}} + \mu_2, \tag{45}$$

where μ_2 is given by (B17). The results in (44) and (45) show that as $-\Gamma/\hbar$ increases, the dimensional eigenfrequencies approach $\zeta_{\min}/2$, no matter where $\zeta_{\min} = \Gamma\Delta_m/a^2$ is located in r.

5. The initial value problem for a Rankine vortex

We now consider the initial value problem in which an impulsive wind stress with infinite horizontal scale sets the uppermost layer of the ocean into unidirectional motion in the zonal direction, and the geostrophic flow is a Rankine vortex. The initial condition for (6) is

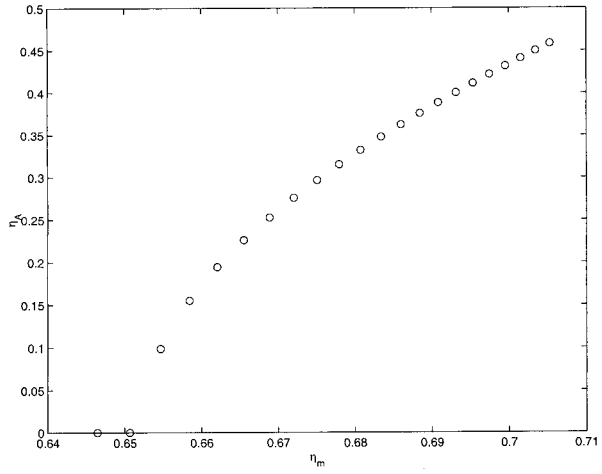

FIG. 10. The value of η at which $A(\eta)$ attains its maximum, η_A, plotted against the value of η at which $\Delta(\eta)$ attains its maximum, η_m.

$LA = u_I(z)$ where u_I is some function concentrated near the surface [an example is given in Balmforth et al. (1998)]. We use the parameter values of Table 1 to define the vertical modes.

The initial condition is then projected onto the vertical normal modes defined in (7) and consequently the initial value problem reduces to solving (10) with an initial condition

$$\mathcal{A}_n(r, \theta, 0) = 1. \tag{46}$$

[Because the problem is linear, we can multiply this solution by the appropriate projection coefficient of $u_I(z)$ onto $\hat{p}_n$.] In order to deal with quantities that decay at large distances from the vortex, it is convenient to define $\mathcal{B}_n = \mathcal{A}_n - 1$. It then follows from (10) that

$$\mathcal{B}_{nt} + \frac{\partial(\Psi, \mathcal{B}_n)}{\partial(x, y)} + \frac{i}{2}Z\mathcal{B}_n - \frac{i\hbar_n}{2}\nabla^2\mathcal{B}_n = -\frac{i}{2}Z, \tag{47}$$

with the initial condition that $\mathcal{B}_n = 0$. The right-hand side of (47) is independent of θ and consequently the solution of (47) is independent of θ; thus the Jacobian term in (47) is zero.

For fixed vertical mode number, n, there are only a finite number of radial modes (Fig. 3); for example, for $n = 10$, there are three trapped radial modes. This situation is similar to other problems in wave guide theory in which the trapped modes do not form a complete set. Consequently, one must also use radiation modes to represent the initial condition. Thus, our solution of (47) is

$$\mathcal{B}_n(r, t) = \sum_{q=0}^{Q(n)} \Phi_n^{(q)} e^{-i\omega_n^{(q)}t} A_n^{(q)}(r) + \mathcal{B}^{(bc)}(r, t), \tag{48}$$

where $\Phi_n^{(q)}$ is defined by

$$2\omega_n^{(q)}\Phi_n^{(q)} = \frac{\displaystyle\int_0^\infty A_n^{(q)}(r)Z(r)r\, dr}{\displaystyle\int_0^\infty rA_n^{(q)2}\, dr}. \tag{49}$$

The number of discrete radial modes for vertical mode n is $Q(n)$.

Because the discrete modes are not complete, the full solution of (47) requires the use of the continuous spectrum and this produces the term $\mathcal{B}^{(bc)}$ in (48). The Laplace transform is a systematic way of obtaining this solution, and using this method, $\mathcal{B}^{(bc)}$ corresponds to a ''branch cut'' contribution in the inversion formula. The full details of the solution for the Rankine vortex are given in appendix C.

It turns out that, for the Rankine vortex, the integrals in (49) can be evaluated analytically; this leads to

$$\Phi_n^{(q)} = \frac{\zeta_c}{\omega_n^{(q)}} \frac{J_1}{\alpha J_0} \frac{J_0^2 K_0^2}{J_1^2 K_0^2 + K_1^2 J_0^2}, \tag{50}$$

where $J_1 = J_1(\alpha)$, $J_0 = J_0(\alpha)$, $K_0 = K_0(\beta)$, and $K_1 = K_1(\beta)$ with

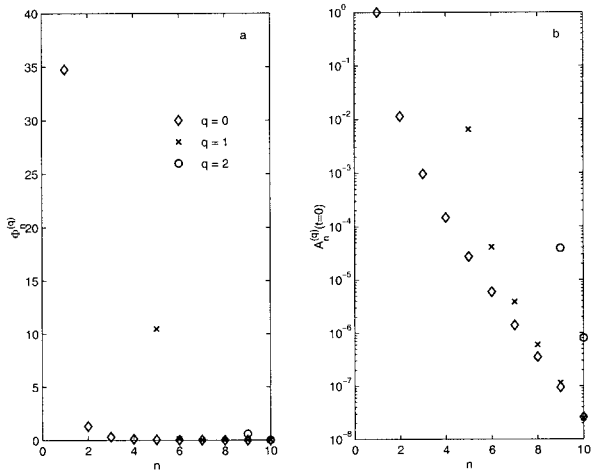

FIG. 11. (a) Projection coefficient, $\Phi_n^{(q)}$, for the lower radial and vertical modes. Vertical modes $n = 1$–6 and radial modes $q = 0$–2 are shown. (b) Amplitude coefficients, $\mathcal{A}_n^{(q)}(t = 0)$, for the Balmforth et al. (1998) initial condition $u_I(z)$. A logarithmic scale is used, normalized with respect to the (0, 0) mode.

$$\alpha = \sqrt{2a^2\omega_n^{(q)}/\hbar_n - \Gamma/\pi\hbar_n}, \tag{51}$$

$$\beta = \sqrt{-2a^2\omega_n^{(q)}/\hbar}. \tag{52}$$

The coefficient $\zeta_c/\omega_n^{(q)}$ may be rewritten as $2\Gamma/\pi\hbar_n\sigma_n^{(q)}$, which shows that it only depends on the parameters used in section 3.

Radial mode $q = 1$ has a large projection coefficient for vertical mode $n = 5$. However, the vertical dependence for the initial condition must be specified to see whether the higher modes will actually be significantly represented in practice. Using the initial condition of Balmforth et al. (1998) [their Eq. (4.4)], the actual projection amplitudes of the modes can be calculated for each n and q using

$$u_I(z) = \sum_n \epsilon_n\sigma_n\hat{p}_n(z) = -\sum_n \mathcal{A}_n\hat{p}_n(z)/R_n^2, \tag{53}$$

where $\epsilon_n = \exp(-n^2/600)$ is a filter to avoid Gibbs-type phenomena and the σ_n are properties of the Gill buoyancy profile. Normalizing with respect to the (0, 0) mode, the next highest amplitudes are the gravest radial mode of the vertical mode $n = 5$, $\mathcal{A}_5^{(0)} = 0.0114$, and the first radial mode of the lowest vertical mode $\mathcal{A}_0^{(1)} = 0.065$. Hence if anything beyond the gravest mode (radial and vertical) is seen, the first radial mode will be observed too. Figure 11 shows the projection coefficient for the first radial and vertical modes, as well as the actual values for the initial amplitudes of the modes $\mathcal{A}_n^{(q)}$.

The remaining part of the solution is the branch cut contribution $\mathcal{B}^{(bc)}(r, t)$. It is impossible to invert the Laplace transform and obtain an exact expression for $\mathcal{B}^{(bc)}(r, t)$. However, there is a simple asymptotic ap-

proximation that is valid if r is fixed and at long times $\hbar_n t/a^2 \gg 1$:

$$\mathcal{B}^{(bc)}(r, t) \sim -1 - \frac{2}{\ln i\tau}\mathcal{J}(\eta) + O\left(\frac{1}{(\ln i\tau)^2}\right), \quad (54)$$

where the function $\mathcal{J}(\eta)$ is defined in (C9) and the nondimensional time τ in (C12). Thus, at fixed r, the continuum contribution in (54) is a very slowly decaying $(\ln t)^{-1}$ transient. This decay is so slow that for all practical purposes it is probably unobservable; this greatly complicates the interpretation of observations, such as those of KST. Thus, while it is true that large-scale forcing will excite the undamped trapped modes [the sum from $q = 1$ to $\mathcal{Q}$ on the right-hand side of (48)], the forcing also produces the long-lived transient in (54). Nevertheless, KST observed intensified near-inertial motions. One reason for the slow decay of the present result is that it effectively produces inertial waves of infinite extent. Adding further physical processes such as realistic forcing or including the β effect would lead to more rapid decay, although the problem would no longer be tractable. In addition, the present barotropic model does not allow for amplification in a vertical critical layer at the base of the ring.

Adding to the possibility of confusion between the discrete modes and the continuum is the fact that the spatial structure of the transient, $\mathcal{B}^{(bc)}(r, t)$, resembles the $q = 0$ mode, although with the wrong frequency to be a normal mode. The radial structure of the continuous spectrum for large time is similar to the normal modes with zero frequency, although the value of $\Gamma/\pi\hbar$ is now arbitrary. This is not true for large r however: when $\eta \equiv r/a > 1$, the $\ln\eta$ term gives the (mistaken) impression that $\mathcal{B}^{(bc)}(r, t)$ grows at great distances from the vortex center. However, the asymptotic approximation in (54) is valid only with r fixed and $t \to \infty$. In order to obtain an expression that is useful when r and t are large, we must take a distinguished limit in which the similarity variable

$$\xi \equiv \frac{r}{\sqrt{\hbar_n t}} \quad (55)$$

is held fixed and $t \to \infty$. One can develop this alternative approximation using the Laplace transform solution in appendix C. But there is a simpler approach that, because of the probable importance of $\mathcal{B}^{(bc)}(r, t)$, is worth developing in the body of this paper.

The basic idea is that at long times and great distances from the vortex many details of the internal structure of the solution become irrelevant and instead one obtains a self-similar evolution. Rewriting (47) in the region outside the vortex (where $Z = 0$) using ξ and τ [defined in (C12)] as new independent variables gives

$$-2i\tau\mathcal{B}_{n\tau} = \mathcal{B}_{n\xi\xi} + \left(\frac{1}{\xi} - i\xi\right)\mathcal{B}_{n\xi}. \quad (56)$$

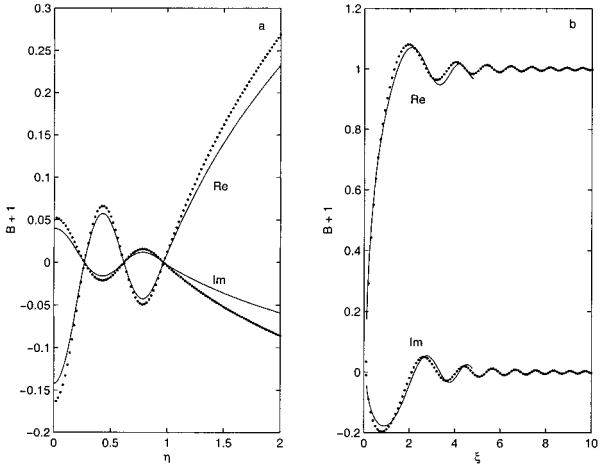

FIG. 12. Real and imaginary parts of the branch cut contribution (solid curves), $\mathcal{B}^{(bc)} + 1$, to the solution of the initial value problem for the Rankine vortex, at time $t = 100 \times (2a^2/\hbar)$. The dotted curves are the asymptotic approximations (54) in the left-hand panel and (59) in the right-hand panel. In this calculation $\Gamma/\pi\hbar = -80$.

With hindsight from the Laplace transform solution of appendix C, we look for a solution of (56) that has the form

$$\mathcal{B}_n = \sum_{m=1}^{\infty} \frac{\mathcal{B}_n^{(m)}(\xi)}{(\ln i\tau)^m}. \quad (57)$$

The leading order term, $\mathcal{B}_n^{(0)}$, satisfies (56) with the left-hand side replaced by zero; the solution of this equation, which decays to zero as $\xi \to \infty$, is

$$\mathcal{B}_n^{(0)} = C\int_{\xi}^{\infty} e^{iu^2/2}\frac{du}{u} = \frac{C}{2}E_1(-i\xi^2/2), \quad (58)$$

where E_1 is the exponential integral. The constant of integration, C, is determined by matching the outer solution in (58) with the inner solution in (54); one finds that $C = -2$. Hence, the similarity solution is given by

$$\mathcal{B}_n = -\frac{E_1(-i\xi^2/2)}{\ln i\tau} + O\left(\frac{1}{(\ln i\tau)^2}\right). \quad (59)$$

Figure 12 shows the asymptotic approximations (54) and (59) for $t = 100 \times (2a^2/\hbar)$. The agreement between the actual solution and the asymptotic approximation is very good for $\eta < 1$ and $\xi = O(1)$. Between these two ranges; that is, on the right-hand edge of the first panel, the agreement is not so good because (54) is not formally valid as r becomes large. The z-dependence enters implicitly into these results through $\hbar$.

6. Discussion

We have examined the $m = 0$ part of the near-inertial eigenspectrum of compact vortices. Normal modes exist for vortices with negative vorticity and relate the two

nondimensional quantities $\Gamma/\hbar$ and σ. Modes appear with the inertial frequency as the nondimensional strength of the vortex $|\Gamma|/\hbar$ grows and become progressively more subinertial as $|\Gamma|/\hbar$ increases. For a fixed value of $\Gamma/\hbar$, higher modes are less tightly bound to the core of the vortex. There is also a continuous radiation spectrum that must be considered for the initial value problem.

For the warm core ring considered by KST and KB, the nondimensional strength of the vortex is large enough for the asymptotic approximation $\omega \approx f_0 + \frac{1}{2}\zeta_c$ to hold. This means that the NIO approximation gives good answers, and the results agree well with KST and KB. For the mode trapped over Fieberling Guyot, the conditions of validity of the NIO approximation do not hold so well since the core vorticity of the flow is no longer small compared to the inertial frequency, and the timescale separation between the inertial oscillation and the slower motion due to the modulation of the NIO is no longer pronounced. Nevertheless, the calculated frequency agrees well with the observed frequency of the diurnal tide.

The modes trapped on a family of smooth vorticity profiles that vanish outside a vortex core have also been calculated. The results are similar to the case of the Rankine vortex. In particular, asymptotic approximations are presented for small and large values of $|\Gamma|/\hbar$. For large $|\Gamma|/\hbar$, the frequency of the trapped mode tends to $\frac{1}{2}\zeta_c$. Provided the core vorticity is smaller than the inertial frequency, this verifies the NIO approximation a posteriori.

The solution to the initial value problem for the Rankine vortex with a spatially uniform initial condition has also been considered. The discrete response is not just concentrated in the lowest radial modes and there is a potentially significant response in the second radial mode. Whether this is actually relevant depends on the initial condition: for the Balmforth et al. (1998) profile, the maximum amplitude for the second radial mode is less than 1% of the lowest radial mode, so it is unlikely to be significant, although it is of the same order as the amplitude of the $n = 1$ vertical mode. Therefore the response for vertical modes greater than $n = 1$ is strongly affected by the first radial mode.

The continuous spectrum is necessary in addition to the discrete spectrum to obtain the full solution. The continuous spectrum decays very slowly in time, like $(\ln t)^{-1}$, and has an oscillatory spatial structure in the core of the vortex that depends only on $\Gamma/\pi\hbar$, whereas the asymptotic behavior far from the vortex has a similarity form in terms of the exponential integral and also decays slowly in time. To a certain extent, some of these features may be due to the simplifications adopted in the present model, but they provide some explicit results for the time-dependent problem.

Acknowledgments. The majority of this work was carried out at the Scripps Institution of Oceanography where the author was funded by a Lindemann Trust Fellowship administered by the English Speaking Union. The support of Queens' College, Cambridge, in the form of a Research Fellowship is also recognized. The advice and guidance of Professor W. R. Young were invaluable. The comments of an anonymous referee were also very helpful. NSF Grant OCE-96-16017 is acknowledged.

APPENDIX A

The $q = 0$ Eigenbranch for $|\Gamma|/\hbar \ll 1$

The confluence as $-\Gamma/\hbar \to 0$ of the $q = 0$ eigencurves in Fig. 7 suggests that there is a general result, independent of the details of the vorticity profile, for the structure of the eigencurves near $(\Gamma/\hbar, \sigma) = (0, 0)$. Consider then a general vorticity profile $\Delta(\eta)$. The scalings of (35) suggest writing Eq. (15) in the form

$$A_{\eta\eta} + \frac{1}{\eta}A_\eta - \sigma A - \frac{\alpha}{\ln\sigma}\Delta(\eta)A = 0, \qquad \text{(A1)}$$

where the circulation, Γ, is related to the unknown function $\alpha(\sigma)$ by

$$\frac{\Gamma}{\hbar} = \frac{\alpha(\sigma)}{\ln\sigma}. \qquad \text{(A2)}$$

The goal is to determine α by expanding (A1) and (A2) in terms of $(\ln\sigma)^{-1}$; that is, $\alpha = \alpha_0 + (\ln\sigma)^{-1}\alpha_1 + \cdots$. It turns out that this expansion is not uniformly valid in η and we will need to introduce an outer coordinate $\rho = \sigma^{1/2}\eta$ and perform an asymptotic match.

In the inner field, the expansion of (A1) has the form $A = A_0 + (\ln\sigma)^{-1}A_1 + \cdots$, and thezeroth-order equation is given by

$$A_{0\eta\eta} + \frac{1}{\eta}A_{0\eta} = 0. \qquad \text{(A3)}$$

The solution may be scaled arbitrarily so we take

$$A_0 = 1. \qquad \text{(A4)}$$

The next order in the expansion of (A1) is $(\ln\sigma)^{-1}$ and at that order

$$A_{1\eta\eta} + \frac{1}{\eta}A_{1\eta} - \alpha_0\Delta(\eta)A_0 = 0. \qquad \text{(A5)}$$

The solution of the equation above can be obtained as a double integral of $\Delta(\eta)$ (or, equivalently, A_1 is proportional to the geostrophic streamfunction Ψ). However, it turns out that all we need for the purposes of matching is the behavior of A_1 when η is large:

$$A_1 \sim \alpha_0\frac{\ln\eta}{2\pi}, \qquad \text{(A6)}$$

where the normalization condition (19) has been used. Assembling the results in (A4) and (A5) we now have the outer limit of the inner expansion: $A \sim 1 + (\alpha_0 \ln\eta/2\pi \ln\sigma)$.

In terms of the outer variable $\rho = \sigma^{1/2}\eta$ the eigenproblem is

$$A_{\rho\rho} + \frac{1}{\rho}A_\rho - A - \frac{\alpha}{\sigma \ln\sigma}\Delta(\sigma^{-1/2}\rho)A = 0. \quad \text{(A7)}$$

For a localized geostrophic eddy, the Δ term will be exponentially small in σ and hence does not enter into the far-field problem. The scaling of A in the far field must now be specified; to match the inner solution we must solve the equation above by taking $A = (\ln\sigma)^{-1}A_0 + A_1 + \cdots$;that is, the outer expansion starts at $(\ln\sigma)^{-1}$. Then the leading-order equation is given by

$$A_{0\rho\rho} + \frac{1}{\rho}A_{0\rho} - A_0 = 0, \quad \text{(A8)}$$

with solution

$$A_0 = pK_0(\rho), \quad \text{(A9)}$$

where p is an unknown constant. We take the inner limit of the outer expansion using $K_0(\rho) \sim -\ln\rho$ as $\rho \to 0$. Thus the inner expansion of the outer solution is $A \sim -(p/2) - p(\ln\eta/\ln\sigma)$.

Matching the two expansions above gives the two relations $p = -2$ and $\alpha_0 = 4\pi$. Thus, the dependence of the eigenvalue σ on the vortex strength parameter $\Gamma/\hbar$ is given by (35) for all localized vorticity distributions.

APPENDIX B

The Eigenvalue Relation in the Case $|\Gamma|/\hbar \gg 1$ and $\sigma \gg 1$

We first consider vorticity profiles that decay monotonically from a central maximum at $\eta = 0$ (the cases with $\Delta_0 > 3\pi/2$ in Fig. 6). Then the profile function $\Delta(\eta)$ has a Taylor expansion of the form

$$\Delta(\eta) = \Delta_0 - \frac{1}{2}\Delta_2\eta^2 + \frac{1}{24}\Delta_4\eta^4 + \cdots, \quad \text{(B1)}$$

where $\Delta_2 = -\Delta''(0) > 0$. [We assume that there are no odd terms in the expansion of $\Delta(\eta)$.] The calculation is insensitive to the presence of an annulus of positive vorticity: it is the location of the negative vorticity maximum that counts.

For large $|\Gamma|/\hbar$, the NIO equation can be rewritten as

$$\epsilon^2\left(A'' + \frac{1}{\eta}A'\right) - \epsilon^2\sigma A + \Delta(\eta)A = 0, \quad \text{(B2)}$$

where $\epsilon^2 \equiv -\hbar/\Gamma$. Equation (36) shows that for the Rankine vortex the leading order behavior is $\sigma \sim -\Delta_0\Gamma/\hbar$, where $\Delta_0 = 1/\pi$ is the value of $\Delta(\eta)$ at the origin. This observation suggests the scaling $\epsilon^2\sigma = \Delta_0 + \mu$, where $\mu = \epsilon\mu_1 + \epsilon^2\mu_2 + \cdots$.Then, using the definition $\tilde{\Delta}(\eta) \equiv \Delta_0 - \Delta(\eta)$, (B2) becomes

$$\epsilon^2\left(A'' + \frac{1}{\eta}A'\right) - \tilde{\Delta}(\eta)A - \mu A = 0. \quad \text{(B3)}$$

The function $\tilde{\Delta}(\eta)$ increases monotonically from zero at $\eta = 0$ to Δ_0 at $\eta = \infty$.

The WKB substitution $A = \exp(S/\epsilon)$ leads to

$$S'^2 - \tilde{\Delta} + \epsilon S'' + \epsilon\frac{1}{\eta}S' - \mu_1\epsilon - \mu_2\epsilon^2 + \cdots = 0. \quad \text{(B4)}$$

However, this equation need not be solved in its entirety. All that is needed is to determine the eigenvalue μ by removing potential singularities in S (arising from the S'/η term) that cannot match onto the regular solution of (B2) near the origin. Expanding the leading-order WKB solution, $S_0' = -\tilde{\Delta}(\eta)^{1/2}$, about the origin gives

$$S_0 \sim -\frac{\sqrt{2\Delta_2}}{4}\eta^2 + \frac{\Delta_4}{96\sqrt{2\Delta_2}}\eta^4 + \cdots. \quad \text{(B5)}$$

Provided Δ_2 does not vanish, the next order equation near the origin is

$$S_1' \sim -\frac{1}{\eta} - \frac{\mu_1}{\sqrt{2\Delta_2}\eta} + \cdots. \quad \text{(B6)}$$

To avoid a singular solution, the next order correction to the eigenvalue must be

$$\mu_1 = -\sqrt{2\Delta_2}. \quad \text{(B7)}$$

Proceeding analogously at the next order gives

$$\mu_2 = \frac{\Delta_4}{6\Delta_2}. \quad \text{(B8)}$$

Assembling the results above, we obtain (44).

We now turn to the case in which the vorticity profile has a maximum, Δ_m, at $\eta = \eta_m \neq 0$ (the cases with $\Delta_0 < 3\pi/2$ in Fig. 7). Define $\tilde{\Delta}(\eta) = \Delta_m - \Delta(\eta)$. The function $\tilde{\Delta}(\eta)$ has a global minimum at η_m and in the neighborhood of this point,

$$\tilde{\Delta} = \frac{1}{2}\tilde{\Delta}_m''(\eta - \eta_m)^2 + \cdots, \quad \text{(B9)}$$

where $\tilde{\Delta}_m'' \equiv -\Delta''(\eta_m) > 0$. Scaling the eigenvalue as $\epsilon^2\sigma = \Delta_m + \mu$, we again obtain the eigenproblem in the form (B3).

In this case the approximate solution is obtained by arguing that the eigenfunction is localized in the neighborhood of η_m and is exponentially small away from this point. A local approximation of (B3) is obtained by defining

$$z = (\eta - \eta_m)/\epsilon^{1/2}. \quad \text{(B10)}$$

In this case, the parameter μ will have the form $\mu = \epsilon\mu_1 + \epsilon^{3/2}\mu_{3/2} + \epsilon^2\mu_2 + \cdots$.Then, at leading order, (B3) is

$$A_{0zz} + \left(-\mu_1 - \frac{1}{2}\tilde{\Delta}_m''z^2\right)A_0 = 0. \quad \text{(B11)}$$

The equation above is the well-known problem of the quantum simple harmonic oscillator. The requirement

that A decays exponentially for large $|z|$ determines the eigenvalue as

$$\mu_1 = -(2q + 1)\sqrt{\tilde{\Delta}''_m/2}, \tag{B12}$$

where q is an integer. We consider only the $q = 0$ branch. Thus

$$A_0 = e^{\mu_1 z^2/2}. \tag{B13}$$

The equation at next order is

$$A_{1zz} + \left(-\mu_1 - \frac{1}{2}\tilde{\Delta}''_m z^2\right)A_1 = -\frac{A_{0z}}{\eta_m} + \mu_{3/2}A_0 + \frac{1}{6}\tilde{\Delta}'''z^3A_0. \tag{B14}$$

Both sides of this equation must vanish when multiplied by A_0 and integrated over all z. Using this compatibility condition, $\mu_{3/2} = 0$. The solution for A_1 is

$$A_1 = \left\{\frac{\tilde{\Delta}'''}{36\mu_1}z^3 + \left[-\frac{\tilde{\Delta}'''}{12\mu_1^2} - \frac{1}{2\eta_m}\right]z\right\}e^{\mu_1 z^2/2}. \tag{B15}$$

The next equation in the hierarchy is

$$A_{2zz} + \left(-\mu_1 - \frac{1}{2}\tilde{\Delta}''_m z^2\right)A_2 = -\frac{A_{1z}}{\eta_m} + \frac{zA_{0z}}{\eta_m^2} + \mu_2 A_0 + \frac{1}{6}\tilde{\Delta}'''z^3A_1 + \frac{1}{24}\tilde{\Delta}^{iv}z^4A_0. \tag{B16}$$

Now the compatibility condition gives

$$\mu_2 = \frac{1}{4\eta_m^2} + \frac{11\tilde{\Delta}'''^2}{576\mu_1^4} - \frac{\tilde{\Delta}^{iv}}{32\mu_1^2}. \tag{B17}$$

APPENDIX C

Solution of the Initial Value Problem for the Rankine Vortex

Equation (47) may be solved using the Laplace transform

$$\tilde{\mathcal{B}}_n(\eta, s) = \int_0^\infty \mathcal{B}_n(\eta, t)e^{-st}\,dt. \tag{C1}$$

Hereafter in this appendix we drop the subscript n. Then, recalling that the solution depends only on η, the transformed version of (47) is

$$s\tilde{\mathcal{B}} + \frac{i}{2}Z\tilde{\mathcal{B}} - \frac{i\hbar_n}{2a^2}\nabla^2\tilde{\mathcal{B}} = -\frac{i}{2s}Z. \tag{C2}$$

For $\eta > 1$, so that $Z = 0$, the solution to (C2) is

$$\tilde{\mathcal{B}}(\eta, s) = \frac{\Gamma}{s(\Gamma - 2\pi a^2 is)}\frac{jJ_1(j)K_0(k\eta)}{kK_1(k)J_0(j) - jJ_1(j)K_0(k)} \tag{C3}$$

and for $\eta < 1$, so that $Z = \Gamma/\pi a^2$, the solution is

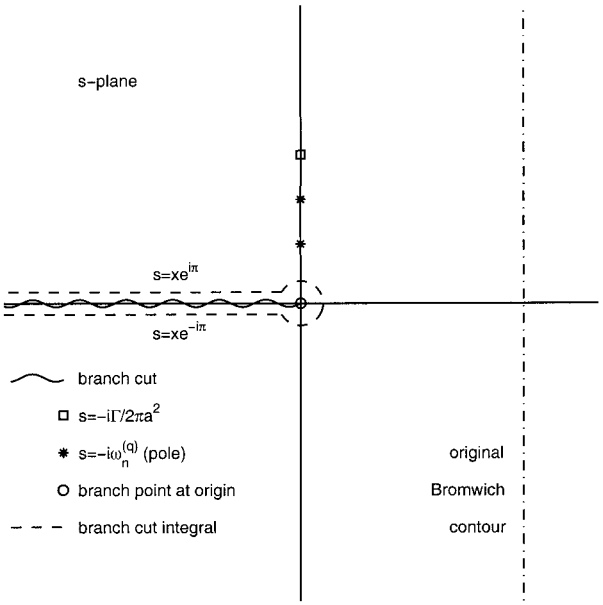

FIG. C1. Complex s-plane for the definition of the Laplace inversion of (C3) and (C4).

$$\tilde{\mathcal{B}}(\eta, s) = \frac{\Gamma}{s(\Gamma - 2\pi a^2 is)}\left[-1 + \frac{kK_1(k)J_0(j\eta)}{kK_1(k)J_0(j) - jJ_1(j)K_0(k)}\right], \tag{C4}$$

where

$$j \equiv \sqrt{\frac{2isa^2}{\hbar} - \frac{\Gamma}{\pi\hbar}}, \qquad k \equiv \sqrt{-\frac{2isa^2}{\hbar}}. \tag{C5}$$

The point $s = 0$ is a branch point; the points in the complex s plane at which $kK_1(k)J_0(j) - jJ_1(j)K_0(k) = 0$ are simple poles (these are simply the points $s = -i\omega_n^{(q)}$). The point $s = -i\Gamma/2\pi a^2$ does not have any special characteristics: the corresponding singularity in (C3) and (C4) is removable.

The Laplace transform is inverted according to the standard prescription,

$$\mathcal{B}(\eta, t) = \frac{1}{2\pi i}\int_{\mathcal{L}} \tilde{\mathcal{B}}(\eta, s)e^{st}\,ds, \tag{C6}$$

where $\mathcal{L}$ is the straight line labeled ''original Bromwich contour'' in Fig. C1. An alternate path of integration is obtained by deforming the contour to the left so that the poles on the imaginary axis are enclosed and evaluated as residues while the remainder of the contour surrounds the branch line along the negative real axis. The residue contribution from the poles gives the sum from $q = 0$ to Q in (48). The contribution from the branch cut gives the remaining term $\mathcal{B}^{(bc)}$.

The $t \gg 1$ behavior of the $\mathcal{B}^{(bc)}$ may be obtained from

(C3), (C4) by an expansion in s near the origin. Expansion of (C3) and (C4) gives

$$\tilde{\mathcal{B}}(\eta, s) + \frac{1}{s}\left[-1 + \frac{\mathcal{J}(\eta)}{\mathcal{J}_1 + \gamma + \ln(k_0/2) + 1/2 \ln s}\right] + O\left(\frac{1}{s^2}\right). \tag{C7}$$

In this expression, $\gamma = 0.577\ldots$ is Euler's constant,

$$j_0 \equiv \sqrt{-\frac{\Gamma}{\pi\hbar}}, \qquad k_0 \equiv \sqrt{-\frac{2ia^2}{\hbar}} \tag{C8}$$

and

$$\mathcal{J}(\eta) \equiv \begin{cases} \dfrac{J_0(j_0\eta)}{j_0 J_1(j_0)}, & \text{if } \eta < 1 \\ \dfrac{J_0(j_0)}{j_0 J_1(j_0)} - \ln\eta, & \text{if } \eta > 1. \end{cases} \tag{C9}$$

In addition $\mathcal{J}_1 \equiv \mathcal{J}(1)$. Logarithmic terms have been grouped in with algebraic terms of the same order in s^{-1}.

The branch cut integral (including the contribution from the singularity at the origin) is then

$$\mathcal{B}^{(bc)}(\eta, t) = -1 - \frac{\mathcal{J}(\eta)}{2} \int_0^\infty \frac{e^{-xt}}{x\{(\mathcal{J}_1 + \gamma + \ln(k_0/2) + 1/2 \ln x)^2 + \pi^2/4\}}\, dx + O\left(\frac{1}{t}\right). \tag{C10}$$

Ignoring higher-order terms, this may be rewritten as

$$\mathcal{B}^{(bc)}(\eta, t) = -1 - 2\mathcal{J}(\eta) \int_0^{-i\infty} \frac{e^{-iu\tau}}{u\{(\ln u)^2 + \pi^2\}}\, du, \tag{C11}$$

where

$$\tau \equiv e^{-2(\mathcal{J}_1+\gamma)} \frac{2\hbar t}{a^2}. \tag{C12}$$

The integral in (C11) may be expressed in terms of Ramanujan's function,

$$N(\theta) \equiv \int_0^\infty \frac{e^{-x\theta}}{x\{(\ln x)^2 + \pi^2\}}\, dx, \tag{C13}$$

by changing the contour of integration to the positive real axis. This is permissible because the original integration contour is the negative imaginary axis and may be deformed onto the positive real axis without passing through the pole of the integrand located at $u = -1$. The final result is

$$\mathcal{B}^{(bc)}(\eta, t) = -1 - 2\mathcal{J}(\eta) N(i\tau). \tag{C14}$$

The asymptotic expansion of Ramanujan's integral is given in Bouwkamp (1971) as

$$N(\theta) = \frac{1}{\ln\theta} - \frac{\gamma}{(\ln\theta)^2} + \frac{\gamma^2 + \pi^2/6}{(\ln\theta)^3} + \frac{0.252015810}{(\ln\theta)^4} + \frac{3.996926673}{(\ln\theta)^5} + \cdots. \tag{C15}$$

The derivation of Bouwkamp (1971) is valid only for real arguments of $N(\theta)$. However it can be shown that (C15) actually holds for θ in the right-half complex plane, including on the imaginary axis.

The asymptotic behavior (C14) is not valid for large η and breaks down for $\eta^2 \gg t$. It is easy to deduce the appropriate asymptotic behavior using an appropriate expansion of the inverse Laplace transform (Ritchie and Sakakura 1956). However, as shown in section 5, it is more instructive to work in a similarity variable appropriate for the far field. The logarithmic behavior exhibited by (C14) is also seen in diffusion problems in cylindrical geometry (Carslaw and Jaeger 1959; Ritchie and Sakakura 1956).

REFERENCES

Abramowitz, M., and I. A. Stegun, Eds., 1965: *Handbook of Mathematical Functions.* Dover, 1046 pp.

Balmforth, N. J., S. G. Llewellyn Smith, and W. R. Young, 1998: Enhanced dispersion of near-inertial waves in an idealized geostrophic flow. *J. Mar. Res.*, **56,** 1–40.

Bouwkamp, C. J., 1971: Note on an asymptotic expansion. *Indiana Univ. Math. J.*, **21,** 547–549.

Brink, K. H., 1989: The effect of stratification on seamount-trapped waves. *Deep-Sea Res.*, **36,** 825–844.

——, 1990: On the generation of seamount-trapped waves. *Deep-Sea Res.*, **37,** 1569–1582.

Carslaw, H. S., and J. C. Jaeger, 1959: *Conduction of Heat in Solids.* 2d ed. Oxford University Press, 510 pp.

Dewar, W. K., 1987: Ventilating warm rings: Theory and energetics. *J. Phys. Oceanogr.*, **17,** 2219–2231.

Gill, A. E., 1984: On the behavior of internal waves in the wakes of storms. *J. Phys. Oceanogr.*, **14,** 1129–1151.

Kunze, E., 1985: Near-inertial wave propagation in geostrophic shear. *J. Phys. Oceanogr.*, **15,** 544–565.

——, 1986: The mean and near-inertial velocity-fields in a warm-core ring. *J. Phys. Oceanogr.*, **16,** 1444–1461.

Kunze, E., and R. Lueck, 1986: Velocity profiles in a warm-core ring. *J. Phys. Oceanogr.*, **16,** 991–995.

——, and J. M. Toole, 1997: Tidally driven vorticity, diurnal shear, and turbulence atop Fieberling Seamount. *J. Phys. Oceanogr.*, **27,** 2663–2693.

——, and E. Boss, 1998: A model for vortex-trapped internal waves. *J. Phys. Oceanogr,* **28,** 2104–2115.

——, R. W. Schmitt, and J. M. Toole, 1995: The energy balance in a warm-core ring's near-inertial critical layer. *J. Phys. Oceanogr.*, **25,** 942–957.

Ritchie, R. H., and A. Y. Sakakura, 1956: Asymptotic expansions of solutions of the heat conduction equation in internally bounded cylindrical geometry. *J. Appl. Phys.*, **27,** 1453–1459.

Young, W. R., and M. Ben Jelloul, 1997: Propagation of near-inertial oscillations through a geostrophic flow. *J. Mar. Res.*, **55,** 735–766.